JOURNAL OF GEOPHYSICAL RESEARCH, VOL. 112, D01305, doi:10.1029/2006JD007096, 2007

Nitric acid measurements at Eureka obtained in winter 2001–2002 using solar and lunar Fourier transform infrared absorption spectroscopy: Comparisons with observations at Thule and Kiruna and with results from three-dimensional models

Elham Farahani,[1] H. Fast,[2] R. L. Mittermeier,[2] Y. Makino,[3] K. Strong,[1] C. McLandress,[1] T. G. Shepherd,[1] M. P. Chipperfield,[4] J. W. Hannigan,[5] M. T. Coffey,[5] S. Mikuteit,[6] F. Hase,[6] T. Blumenstock,[6] and U. Raffalski[7]

Received 18 January 2006; revised 21 July 2006; accepted 29 August 2006; published 9 January 2007.

[1] For the first time, vertical column measurements of nitric acid (HNO_3) above Eureka (80.1°N, 86.4°W), Canada, have been made during polar night using lunar spectra recorded with a Fourier transform infrared (FTIR) spectrometer, from October 2001 to March 2002. This site is part of the primary Arctic station of the Network for the Detection of Stratospheric Change. These measurements were compared with FTIR measurements at two other Arctic sites: Thule, Greenland (76.5°N, 68.8°W), and Kiruna, Sweden (67.8°N, 20.4°E). Eureka lunar measurements are in good agreement with solar ones made with the same instrument. Eureka and Thule HNO_3 columns are consistent within measurement error. Differences between HNO_3 columns at Kiruna and those at Eureka and Thule can be explained on the basis of available sunlight hours and location of the polar vortex. The measurements were also compared with results from a chemistry-climate model, the Canadian Middle Atmosphere Model (CMAM), and from a three-dimensional chemical transport model, SLIMCAT. This is the first time that CMAM HNO_3 columns have been compared with observations in the Arctic. The comparison of CMAM HNO_3 columns with Eureka and Kiruna data shows good agreement. The warm 2001–2002 winter with almost no polar stratospheric clouds makes the comparison with this version of CMAM, which has a known warm bias, a good test for CMAM under these conditions. SLIMCAT captures the magnitude of HNO_3 columns at Eureka, and the day-to-day variability, but generally reports higher values than were measured at Thule and Kiruna.

Citation: Farahani, E., et al. (2007), Nitric acid measurements at Eureka obtained in winter 2001–2002 using solar and lunar Fourier transform infrared absorption spectroscopy: Comparisons with observations at Thule and Kiruna and with results from three-dimensional models, *J. Geophys. Res.*, *112*, D01305, doi:10.1029/2006JD007096.

1. Introduction

[2] The first Fourier transform infrared (FTIR) spectrometer measurements of nitric acid (HNO_3) during polar night, using the Moon as the light source, were carried out by Notholt in December 1992 and in February 1993 at the Ny-Alesund Arctic NDSC station (79°N, 12°E) [*Notholt et al.*, 1993, 1995, 1997; *Notholt*, 1994a, 1994b]. At Kiruna, lunar FTIR spectra have been recorded since the winter of 1994–1995 [*Schreiber et al.*, 1997]. This paper reports on the first measurements of HNO_3 vertical columns at Eureka throughout the polar night using the FTIR system with the Moon as the light source. These measurements were made in the winter of 2001–2002 but solar observations have been performed there regularly since 1993. Also, this is the first time that HNO_3 columns measured at the three NDSC Arctic sites, Eureka, Thule and Kiruna, have been intercompared.

[3] HNO_3 observations during polar night provide valuable information about the processes which condition the polar stratosphere for springtime ozone depletion. HNO_3 is the primary constituent of polar stratospheric clouds (PSCs). PSCs provide surfaces for heterogeneous chemistry through which active chlorine (ClO, ClOOCl, OClO) is released from

[1]Department of Physics, University of Toronto, Toronto, Ontario, Canada.
[2]Meteorological Service of Canada, Downsview, Ontario, Canada.
[3]Japan Meteorological Agency, Tokyo, Japan.
[4]Institute for Atmospheric Science, School of Earth and Environment, University of Leeds, Leeds, UK.
[5]Optical Techniques Project, Atmospheric Chemistry Division, National Center for Atmospheric Research, Boulder, Colorado, USA.
[6]Institute of Meteorology and Climate Research, Forschungszentrum Karlsruhe and University of Karlsruhe, Karlsruhe, Germany.
[7]Swedish Institute of Space Physics, Kiruna, Sweden.

0148-0227/07/2006JD007096$09.00

its reservoir species, thereby becoming available to participate in ozone-depleting processes [*Solomon et al.*, 1986; *World Meteorological Organization* (*WMO*), 2003; *Grooß et al.*, 2005]. Additionally, the sedimentation of large HNO_3 particles removes active nitrogen ($NO_x = NO + NO_2$) from the stratosphere and makes conditions more favorable for destruction of ozone by preventing the formation of inactive chlorine reservoirs such as $ClONO_2$ [*WMO*, 2003].

[4] Stratospheric HNO_3 has a winter maximum because of the conversion of NO and NO_2 to N_2O_5 and HNO_3 during periods of darkness. Also HNO_3 abundances increase toward the poles in all seasons, because of the combination of poleward transport and decreasing solar illumination except in regions of PSC formation [*Santee et al.*, 2004]. These two processes contribute to the observed seasonal behavior of HNO_3 at high latitudes [*WMO*, 2003]. However, Arctic measurements show additional features that are specific to conditions inside the Arctic polar vortex.

[5] Here we present the first comparison of the Canadian Middle Atmosphere Model (CMAM) chemical fields with observations in the polar regions, simulated at Eureka and Kiruna. As CMAM is a chemistry-climate model, its years do not correspond to any particular year and the comparison must be statistical in nature. The 2001–2002 winter was relatively warm, with two major stratospheric warmings, one occurring in December 2001 and the second in February 2002, and with the calculated daily average area for PSC occurrence near zero throughout the winter [*Manney et al.*, 2005]. Thus the meteorological conditions for this winter provide an ideal opportunity to compare with observations, in particular to see the seasonal buildup of HNO_3 under conditions of no PSCs, and to test CMAM given the known warm bias of Arctic winters in this version of the model [*Austin et al.*, 2003]. The measurements are also compared with the SLIMCAT chemical transport model, which has been extensively tested in many past polar studies using a range of observations [e.g., *Singleton et al.*, 2005; *Goutail et al.*, 2005; *Davies et al.*, 2005]. In contrast to CMAM, because SLIMCAT is a chemical transport model driven by observed winds and temperatures, it should capture the observed day-to-day variability.

2. Instrumentation

[6] The Bomem DA8 FTIR spectrometer at Eureka has been used with a light-sensitive mirror-tracking system mounted over an opening in the flat roof above the spectrometer laboratory at Eureka since 1993 [*Donovan et al.*, 1997]. In 1999, a side-by-side intercomparison was conducted at the Eureka observatory between the Bomem DA8 FTIR spectrometer and a mobile Bruker M120 FTIR spectrometer, operated by the British National Physical Laboratory (NPL) [*Murphy et al.*, 2001]. The tracking mirror is normally used to reflect sunlight down into the laboratory to fill the input optics of the spectrometer. A small portion of the solar beam is reflected into a sensitive photomultiplier tube that works as a quadrant diode system. The output from the photomultiplier is part of a feedback circuit that activates the elevation and azimuth motors driving the tracking mirror so that the most intense portion of the solar disk is always viewed by the spectrometer. To record atmospheric absorption spectra using the Moon as the light source, the sensitivity of the tracking system was increased by approximately five orders of magnitude over that available with the original system, which was required to track only the Sun. This increase in sensitivity was obtained by employing greater amplification of the signal from the photomultiplier tube. With this higher sensitivity it was easy to track the Moon and record atmospheric absorption spectra even when the Moon was not completely full. The same system was also used for recording absorption spectra using the Sun as the light source, merely by inserting a neutral density filter in front of the tracker photomultiplier tube, so as to compensate for the much brighter Sun. The spectra for measuring HNO_3 were recorded with a mercury-cadmium-telluride (MCT) detector in combination with a 7.4 μm long-pass filter.

3. Eureka Observations

[7] The FTIR campaign started with the recording of atmospheric absorption spectra using the Sun as the light source, as has been carried out at Eureka every fall and late winter/early spring since 1993. The HNO_3 spectra were recorded in the 700 to 1300 cm^{-1} interval at a resolution of 0.004 cm^{-1} with a 3.09 milliradian field of view (FOV). To improve the signal-to-noise ratio (SNR), four interferograms were coadded over a period of 11 min and 40 s for Fourier transformation into one spectrum. Solar spectra were obtained on four clear days in October, just prior to polar sunset on 22 October 2001. The recording of atmospheric spectra for HNO_3 measurements was then continued about a week later when the illumination of the Moon was greater than 80%. This degree of illumination is required in order to fill the field of view of the DA8 spectrometer. Because of the weaker lunar intensity compared to that of the Sun, a lower resolution of 0.02 cm^{-1} and the higher preamplifier gain setting on the MCT detector were used to record the lunar spectra in the 550 to 1350 cm^{-1} interval with a FOV of 7.32 milliradians. The coaddition of 16 lunar interferograms to increase the SNR required 10 min and 18 s to obtain one lunar spectrum. This was followed by the coaddition of 16 sky interferograms, recorded after the tracker was pointed away from the Moon in azimuth only, to produce one sky spectrum. The sky spectrum represented the nonnegligible background spectrum, due to broad-band sky and instrument emission, which was assumed to be superimposed on the lunar spectrum [*Notholt*, 1994a]. The campaign continued until the end of March 2002, typically with four to five clear nights around the full Moon near the end of each month. By the end of February, polar night ended and solar spectra were again recorded. In summarizing the Eureka observations, both solar and lunar FTIR spectra were recorded for a few days and nights at the end of October 2001, prior to polar night when only lunar measurements were made, and again for about three weeks after polar night ended near late February 2002. Solar spectra were then recorded until the end of March.

4. Spectral Analysis

[8] The time corresponding to the average interferogram zero-path difference of a coadded spectrum was used to calculate the astronomical solar zenith angle with an in-house algorithm. The lunar zenith angles were obtained by applying an appropriate algorithm (the U.S. Naval Observatory online

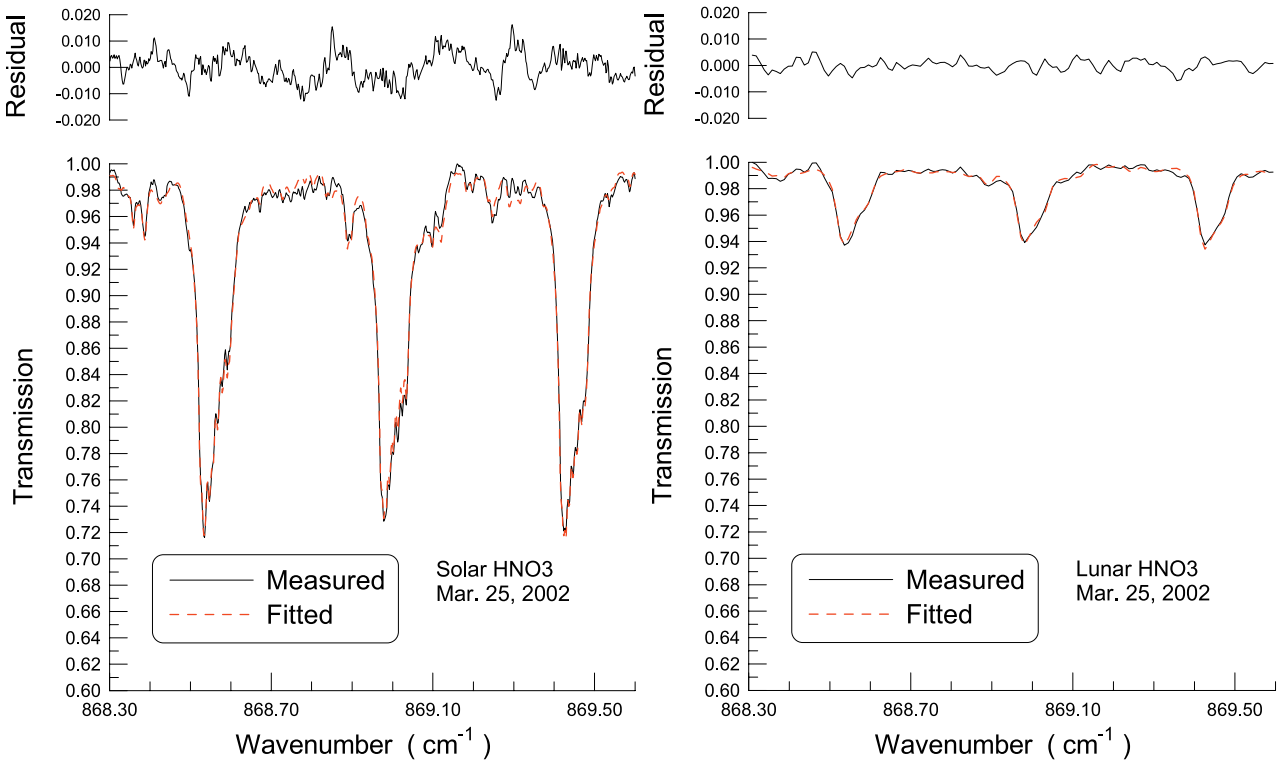

Figure 1. (left) A typical solar HNO_3 spectral fit and its residual. (right) A typical lunar HNO_3 spectral fit and its residual. Both are for spectra recorded with the Eureka FTIR.

resources at: http://aa.usno.navy.mil/). The atmospheric absorption spectra recorded with the MCT detector, using the Sun as the source, exhibited a zero-level offset due to detector nonlinearity. This is seen in the line centers of saturated absorption lines where the intensity level was above zero and is a few percent of the maximum intensity in the spectral region of interest. This zero-level offset was determined by fitting a parabola through the minimum intensity level of several fully absorbed spectral features and then subtracted from the MCT spectra prior to spectral fitting with SFIT1. The saturated features in the solar spectra, in the nitric acid spectral regions, appeared unsaturated in the spectra recorded with the Moon as light source. This was due to the lower resolution of the lunar spectra and the relatively high lunar elevation angles. The zero-level offsets for these spectra, mainly due to self-emission of the instrument, were therefore determined from the sky spectra recorded at the lunar zenith angle immediately after acquiring each lunar spectrum. That is, the continuum intensity level of the sky spectrum was subtracted from the lunar spectrum before spectral fitting with SFIT1.

[9] The retrieval of HNO_3 column amounts from our atmospheric absorption spectra is based on the SFIT1 spectral fitting routine [*Rinsland et al.*, 1982, 1988]. SFIT1.09e was applied to narrow spectral microwindows containing absorption features of the target molecules. The HNO_3 microwindow used is defined as the narrow interval from 868.3 to 869.6 cm^{-1}; typical fits for solar and lunar spectra are seen in Figure 1. To calculate the synthetic spectra with SFIT1, we adopted the line parameters in the HITRAN 1992 compilation [*Rothman et al.*, 1992] plus updates. For comparison, applying the more recent HITRAN 2000 compilation [*Rothman et al.*, 2003] to a sample of our spectra reduces the retrieved HNO_3 vertical columns by only 2%. Our set of a priori volume mixing ratio (VMR) profiles (REFTOON41) is based on low-latitude balloon measurements [*Peterson and Margitan*, 1995] but modified, as described below, for the high-latitude location of Eureka. Temperature, pressure and relative humidity profiles were obtained from radiosondes launched twice daily from Eureka. Above the maximum sonde altitude, the profiles of temperature and pressure are extended to approximately 50 km with data from the U.S. National Center for Environmental Predictions (NCEP). Above 50 km the winter sub-Arctic U.S. Standard Atmosphere is used to 100 km.

[10] The set of VMR a priori profiles used for the solar retrievals were modified with the equation described by *Meier* [1997] to reflect the tropopause height, determined from Eureka radiosondes, and to allow for an atmospheric Degree of Subsidence or Ascent (DOSA) above the tropopause, on the basis of the findings of *Toon et al.* [1992b]. The DOSA parameter was determined by considering N_2O and CH_4 as dynamical tracer molecules, unaffected by atmospheric chemistry during the measurement campaign. SFIT1 was applied to the solar absorption spectra of these target gases by iterating through a sequence of values for the DOSA parameter, scaling the corresponding modified a priori profile until the best fit was achieved and noting the DOSA value for the best spectral fit in the sequence. A daily mean DOSA was then determined by obtaining a daily average from the two tracer gases. This mean DOSA value was then used to modify the a priori VMR profiles for the rest of the gases in the

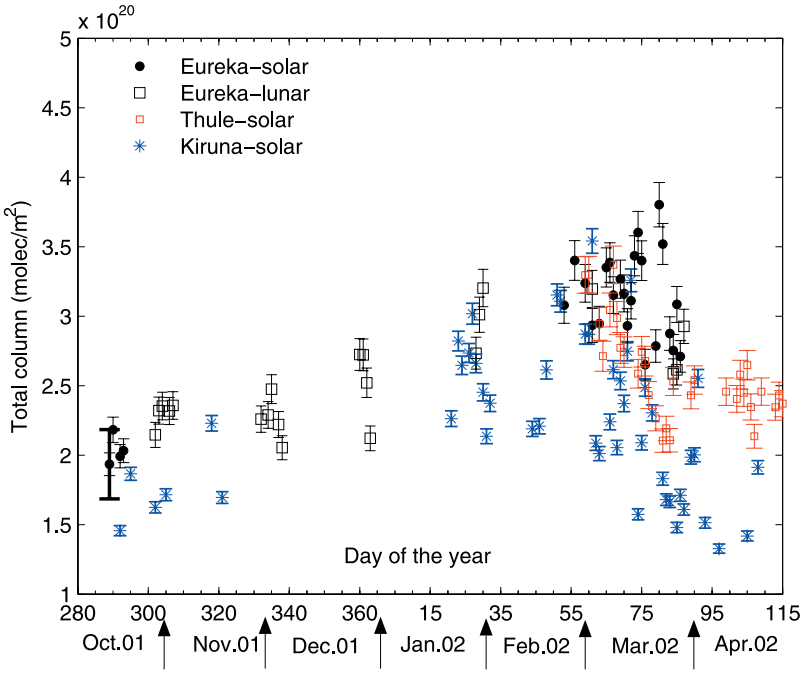

Figure 2. Time series of HNO_3 columns measured at the three Arctic sites, Eureka, Thule, and Kiruna, from October 2001 to April 2002. Error bars indicate random errors. The single large error bar on the first Eureka data point represents the systematic error of 12.9% for Eureka observations. For Thule and Kiruna, the systematic error is 10% (not shown).

REFTOON41 set. The column amounts of the target trace gases were determined by allowing SFIT1 to scale the DOSA-modified a priori profiles in the target gas microwindow until the best fit was attained.

[11] In view of the anticipated large uncertainty in derived DOSA parameters from the lower-resolution lunar spectra, and the time required, the authors decided to omit the DOSA modification of the VMR a priori profiles for the lunar retrievals, with the assumption that it would not significantly affect the retrieved columns. The a priori profiles were only modified by the *Meier* [1997] equation to be consistent with the radiosonde tropopause height and then scaled by SFIT1 to achieve the best fit to the HNO_3 spectral windows. Although subtracting the zero-level offset from the lunar spectra should correct to a large degree for the broad-band intensity offset due to sky and instrument emission, it is also necessary to account for discrete sky emission. We therefore multiplied our lunar-retrieved column amounts by a small correction factor, given by equation (5) of *Notholt and Lehmann* [2003]. The correction factor is approximately equal to the light source irradiance divided by the difference between the light source and sky irradiances. We calculated this factor using an algorithm developed by J. Notholt (private communication, 2001) and found it to be approximately 1.08 for the retrieved Eureka HNO_3 columns.

[12] A mean daily vertical column was calculated from the individual HNO_3 column measurements at Eureka from two or more spectra recorded each day or night. Error estimates of the retrieved column amounts were determined according to the method described by *Murphy et al.* [2001], to account for instrument effects, choice of algorithm, microwindows, line parameters, a priori volume mixing ratio profiles, and uncertainty in the temperature profile. These sources of uncertainty were estimated to be the same for solar and lunar measurements and yield a total error of 13.6%. Of this, 12.9% is attributed to systematic error and 4.2% to random error. Figure 2 shows the time series of HNO_3 mean daily columns from October 2001 to March 2002. The error bars in Figure 2 are the estimate of random error, while the systematic error is shown as a single large error bar on the first data point.

5. Additional Arctic Measurements

[13] The HNO_3 columns observed at Eureka were compared with HNO_3 columns measured at two other Arctic NDSC sites: Thule, Greenland (76.5°N, 68.8°W) and Kiruna, Sweden (67.8°N, 20.4°E). The Thule measurements were obtained from spectra recorded with a 250 cm Optical Path Difference (OPD) Bruker 120M FTIR spectrometer [*Goldman et al.*, 1999]. Currently the autonomously operated Thule FTIR spectrometer records data for ~30% of available days between 21 February and 20 October. In the winter of 2001–2002 Thule HNO_3 measurements were carried out from the end of February to the end of April 2002, using only the Sun as the light source.

[14] The Thule data for the period shown here were analyzed using the SFIT2 v3.82 program which uses a semiempirical optimal estimation algorithm [*Rodgers*, 1976] to perform a point-by-point fitting of the observed spectra with a 41-layer, line-by-line spectral forward model calculation [*Chang and Shaw*, 1977; *Hase et al.*, 2004]. Total column amounts are the integrated retrieved HNO_3 vertical profiles. Two microwindows in the 870 cm^{-1} region from all spectra recorded on a given day (1 to 5 spectra) were used for each daily average column retrieval. The random error on the

daily column measurement is 4% and the systematic component of the error is estimated to be 10%. The forward model uses the HITRAN 2000 database with updates to November 2001 [*Rothman et al.*, 2003] and temperatures from the NCEP analyses [*Lait et al.*, 2005].

[15] FTIR observations have been made at the Swedish Institute of Space Physics in Kiruna since March 1996 within the framework of the NDSC [*Blumenstock et al.*, 2003; *Meier et al.*, 2005] in collaboration with IMK Karlsruhe, IRF Kiruna and the University of Nagoya. Infrared solar absorption spectra are recorded with a Bruker 120 HR FTIR allowing a maximum optical path difference of 360 cm, equivalent to a spectral resolution of up to 0.0025 cm^{-1}. Typically, a spectral resolution of 0.005 cm^{-1} is applied. Spectra are coadded for up to 15 min during noon and 5 min during sunrise and sunset in order to limit the variation of the solar zenith angle to 0.2°. For the winter of 2001–2002 Kiruna reported only solar measurements of HNO_3, during October and November in 2001 and again starting from polar sunrise in January 2002 until the end of April.

[16] The Kiruna FTIR spectra are analyzed with the inversion program PROFFIT (PROFile FIT) [*Hase*, 2000; *Hase et al.*, 2004] using the forward model KOPRA (Karlsruhe Optimized Precise Radiative transfer Algorithm) [*Hopfner et al.*, 1998; *Kuntz et al.*, 1998; *Stiller et al.*, 1998]. The synthetic spectra are calculated using daily pressure and temperature data from NCEP [*Kanamitsu*, 1989]. Spectroscopic data are taken from the HITRAN 2000 database [*Rothman et al.*, 2003]. The inversion code PROFFIT allows the retrieval of vertical profiles from the absorption line shape using the Optimal Estimation Method of Rodgers [*Rodgers*, 1976, 1990], the Phillips-Tikhonov approach [*Phillips*, 1962; *Tikhonov*, 1963], or scaling of a priori profiles in user defined altitude intervals. Two microwindows are fitted simultaneously: 867.0–869.6 and 872.8–875.2 cm^{-1}. Column amounts of HNO_3 measured at Kiruna have been studied for different winters [*Wegner et al.*, 1992; *Blumenstock et al.*, 2003; *Kopp et al.*, 2003]. The precision error for the Kiruna data is 2.5%; there is an additional systematic spectroscopic error of ~10%.

[17] Eureka solar and lunar measurements started in late October 2001 and continued through March 2002, while Thule solar measurements cover the period from the end of February to the end of April 2002. Kiruna reported a few solar measurements during October and November 2001 then resumed solar observations in January 2002 at polar sunrise and HNO_3 measurements until the end of April are included in this paper.

6. Atmospheric Models

[18] Two atmospheric models, CMAM and SLIMCAT, were used for comparison with the measurements. CMAM and SLIMCAT are different types of models and thus the nature of the comparison with the measurements is quite different in the two cases. CMAM is an upward extension of the Canadian Centre for Climate Modeling and Analysis spectral General Circulation Model (GCM) up to 0.0006 hPa (roughly 100 km altitude), described in detail by *Beagley et al.* [1997]. CMAM incorporates radiation, interactive chemistry, gravity wave drag, as well as all the processes in the GCM. The model has a comprehensive representation of stratospheric chemistry [*de Grandpré et al.*, 1997]. A recent comparison of CMAM with other Chemistry-Climate models is provided by *Austin et al.* [2003].

[19] The CMAM version used here, known as version 7, has prognostic variables computed in spectral space using T32 resolution (corresponding to resolution of about 6° in latitude and longitude) and 65 vertical levels (about 2 km vertical resolution in the middle atmosphere). This version also contains a chemical module to account for heterogeneous reactions that occur on stratospheric ternary solutions (STS), and water ice in polar regions without sedimentation; however during this run of CMAM, temperatures at the closest grid point to Eureka (80.3°N, 84.4°W) were not low enough for the heterogeneous module to be activated. For the model comparison presented here, mean HNO_3 columns are generated from CMAM HNO_3 profiles at the closest grid point to Eureka and to Kiruna (the values close to Thule were not saved). The model outputs HNO_3 profiles at every time step, resulting in 144 profiles per day. These profiles are interpolated to a common altitude grid and averaged to obtain daily mean profiles. Daily columns come from integrating these daily mean profiles. Because CMAM is a free-running chemistry-climate model, and here is run under fixed forcing representative of the present day, a given day in the observations cannot be expected to match any particular day in CMAM, but at best be consistent with the ensemble of such days given by 20-year simulations. Thus mean HNO_3 columns result from averaging daily columns for the same day of the year over 20 years of the CMAM simulation, and the standard deviation represents the interannual variability of daily means in the model. The interannual variability in CMAM version 7 is generally underestimated because the quasi-biennial oscillation (QBO), solar variability, and aerosol variability are not included. Also, although this CMAM version adopts climatological sea-surface temperatures (SSTs) which vary from month to month, they stay the same for each year of the model simulations.

[20] SLIMCAT is an off-line 3-D Chemical Transport Model (CTM) which has been widely used in previous studies of stratospheric chemistry (described in detail by *Chipperfield* [1999]). The model has a detailed treatment of stratospheric chemistry. The model temperatures and horizontal winds are specified from analyses and the vertical transport in the stratosphere is diagnosed from radiative heating rates. In the stratosphere the model uses an isentropic coordinate and this has been extended down to the surface using hybrid sigma-theta levels [*Chipperfield*, 2006].

[21] In the SLIMCAT run 323 shown here, the model was integrated with a horizontal resolution of 7.5° × 7.5° and 24 levels extending from the surface to about 55 km. The model was forced by European Centre for Medium Range Weather Forecasts (ECMWF) analyses and the simulation started on 1 January 1977. Above 350 K, where the model used pure theta levels, vertical advection was calculated from heating rates diagnosed using the CCMRAD scheme [*Chipperfield*, 2006]. *Feng et al.* [2005] showed that using this radiation scheme gave a better simulation of vertical transport (i.e., more descent) than the previously used MIDRAD scheme. This improved the modeled polar ozone loss. Below 350 K, vertical motion is calculated from the forcing analyses and the troposphere is assumed to be well mixed.

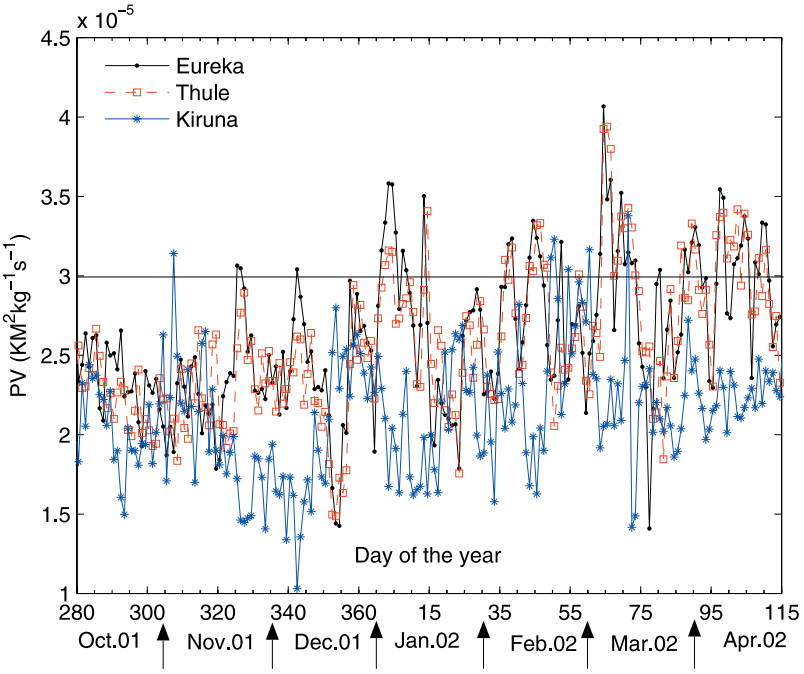

Figure 3. Time series of ECMWF potential vorticity (PV) values at 475 K at Eureka, Thule, and Kiruna, from October 2001 to April 2002. The solid line is at PV = 3.0×10^{-5} $Km^2kg^{-1}s^{-1}$, which is an indication of the edge of the vortex [*Nash et al.*, 1996].

[22] In the SLIMCAT simulation used here, the model halogen loading was specified from observed tropospheric CH_3Br and halon loadings [e.g., *WMO*, 2003] with an additional 6 pptv contribution assumed from short-lived bromine sources. Accordingly, the stratospheric bromine loading near the year 2000 was approximately 21 pptv. Photochemical data were generally taken from paper by *Sander et al.* [2003], except for some details related to polar Cl_2O_2 chemistry [*Feng et al.*, 2005]. Output from the simulation was saved every 2 days at 0000 UT for the location of Eureka.

7. Measurement and Model Comparisons

[23] The daily mean HNO_3 vertical columns for the three Arctic sites are plotted in Figure 2 as a time series from October 2001 to April 2002. For clarity, the error bars shown are just the random component of the total error: 4.2%, 4%, and 2.5% for Eureka, Thule, and Kiruna respectively. To illustrate the relative magnitude of the systematic error, this is shown on the first Eureka data point. From Figure 2, it is evident that solar and lunar observations made at Eureka are in good agreement. HNO_3 columns over Eureka steadily increased from October through to about 15 March, starting near 1.8×10^{20} molec/m^2 and reaching a peak value of approximately 3.5×10^{20} molec/m^2. This observed trend in HNO_3 is consistent with the reduction in HNO_3 photolysis by sunlight and the conversion of NO_x back to N_2O_5 and HNO_3 during periods of darkness which tends to produce more HNO_3 in winter than in summer [*Wood et al.*, 2004]. The HNO_3 column densities and their trend observed at Eureka are also consistent with the lunar FTIR HNO_3 measurements in the winters of 1992–1995 by *Notholt et al.* [1997] over Ny-Alesund, close to Eureka's latitude.

[24] The March 2002 solar and lunar HNO_3 vertical columns at Eureka generally agree with the Thule solar measurements within the error bars. This is consistent with ECMWF potential vorticity (PV) values at 475 K for the same period, shown in Figure 3, which indicates that similar dynamical conditions were experienced at these two sites. The larger differences observed between Eureka and Thule HNO_3 columns on 22 March (day 81) 2002 is due to the relative position of the polar vortex based on ECMWF Northern Hemisphere PV maps at 475 K. For example in Figure 4, on 22 March 2002 (day 81) Eureka is inside the polar vortex while Thule is at the edge of the vortex [*Nash et al.*, 1996]. This explains why on this day, Eureka, located in a high-PV area, observed higher HNO_3 columns typical of the HNO_3-rich air mass inside the polar vortex than did Thule, situated only at the edge of the vortex as shown by the lower PV value. In contrast, on 25 March 2002 (day 84) both Eureka and Thule are at the edge of the polar vortex, as seen in Figure 4, and therefore both report similar lower HNO_3 columns associated with the lower PV values.

[25] The Kiruna solar HNO_3 vertical columns from October to November 2001 and again from January to April 2002 are consistently lower than those measured at Eureka and Thule. This can be attributed to different dynamical conditions experienced at Kiruna compared to the other two sites as shown in Figure 3. That is, Kiruna remained mostly outside the vortex during the observation period. Also Kiruna's latitude is exposed to more sunlight than the higher-latitude stations. This results in more rapid photolysis of HNO_3 to NO_x species at Kiruna than at Eureka and Thule.

[26] Figure 5 presents the measured HNO_3 columns at each of the sites, with systematic errors indicated as discussed in section 5. CMAM climatological HNO_3 columns

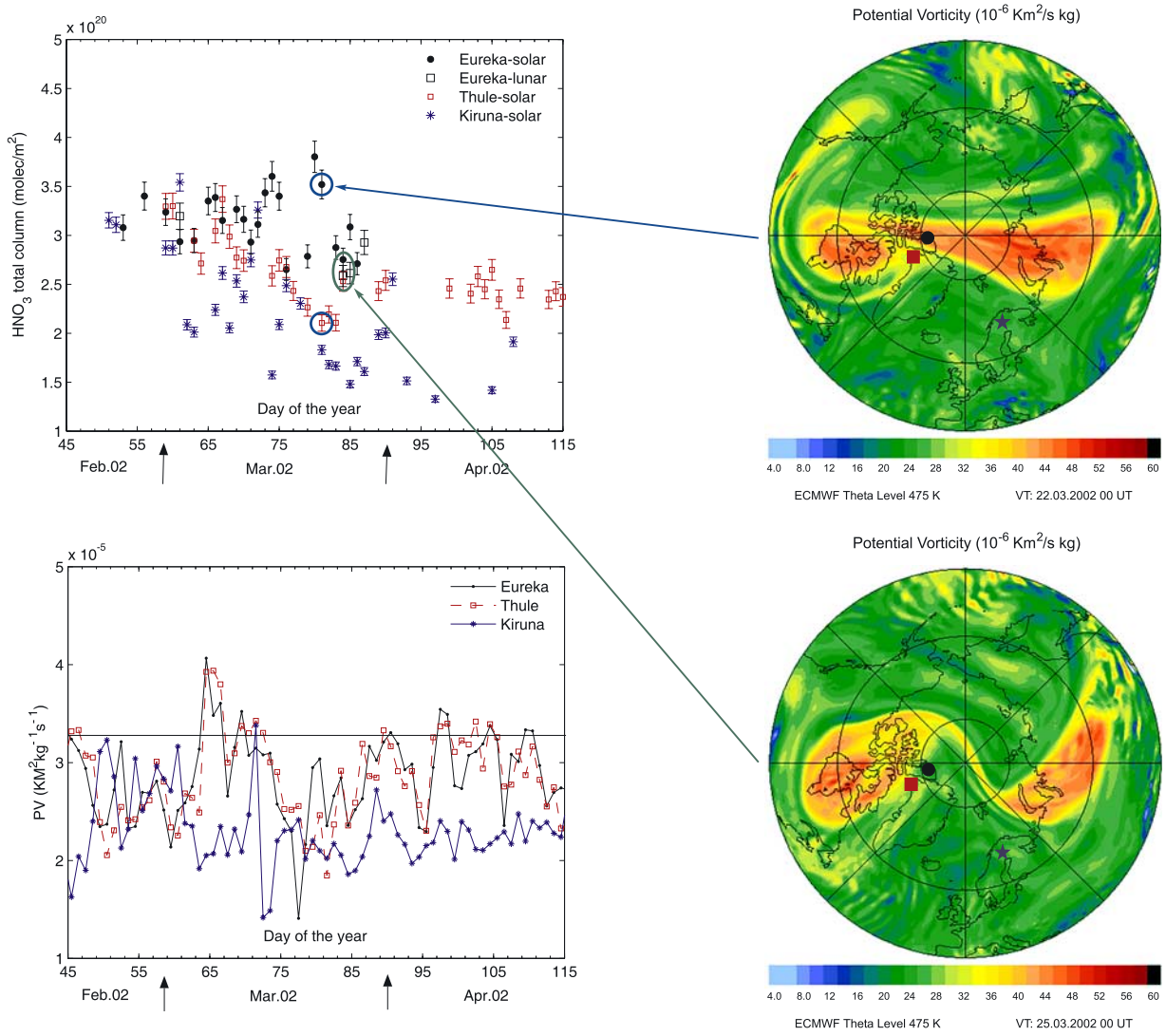

Figure 4. (top left) Observed HNO_3 columns at the three Arctic sites during spring 2002 and (bottom left) ECMWF PV at 475 K. ECMWF global maps of PV at 475 K for (top right) day 81 (22 March 2002) and (bottom right) day 84 (25 March 2002).

at Eureka and Kiruna are also included in Figure 5; this represents the first comparison of CMAM HNO_3 with observations in the polar regions. The CMAM climatological HNO_3 columns at the closest grid point to Eureka show excellent agreement with the Eureka lunar measurements through the winter, with an average difference of 1.9% ((FTIR-CMAM)/FTIR) for the 21 measurement days. The CMAM climatological HNO_3 columns are also in agreement with the Eureka solar measurements during fall 2001 and spring 2002 within the 1σ interannual variability of CMAM (and with an average difference of 12% for 27 days). Combining the lunar and solar results gives an average difference of 7% between CMAM and the FTS measurements. In Figure 3, the ECMWF PV time series shows that Eureka and Thule did not stay inside the polar vortex for any extended period, while Kiruna rarely experienced vortex conditions during the observation period. The climatological nature of CMAM prevents it from capturing the observed day-to-day variations in PV. However, because 2001–2002 was a particularly warm winter, comparisons between the measurements and CMAM provide an excellent opportunity to assess how well the model captures the chemistry under non-PSC conditions. The agreement of CMAM version 7 with the observations is consistent with the lack of cold winters in this version of the model [*Austin et al.*, 2003] and shows the seasonal build up of HNO_3 in the absence of PSCs and denitrification.

[27] The CMAM climatological HNO_3 columns at the closest grid point to Kiruna were compared with solar HNO_3 values measured at Kiruna, also shown in Figure 5. The CMAM climatological HNO_3 columns are consistent with the measured values at Kiruna: 33 out of 51 days are within 1σ variability, even when only the random errors on the Kiruna measurements are considered. This increases to 39 out of 51 days when the 10% systematic error is also taken into account.

[28] In Figure 5, the SLIMCAT 323 output is also compared with the measured HNO_3 vertical columns at Eureka,

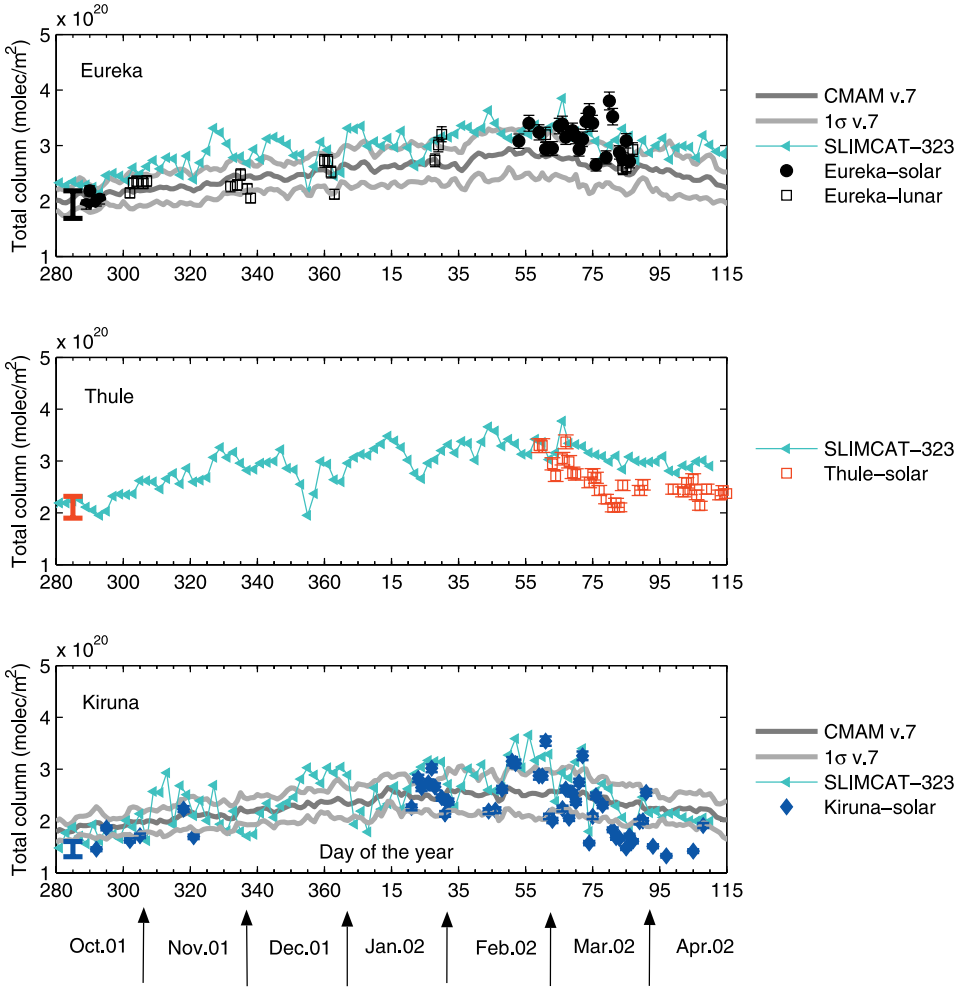

Figure 5. (top) HNO_3 columns measured at Eureka compared with CMAM version 7 chemical fields at the closest grid point to Eureka and with SLIMCAT 323 at Eureka. (middle) HNO_3 columns measured at Thule compared with SLIMCAT 323 at Thule. (bottom) HNO_3 columns measured at Kiruna compared with CMAM version 7 chemical fields at the closest grid point to Kiruna and with SLIMCAT 323 at Kiruna. The CMAM variability range is one standard deviation. Error bars indicate random errors for Eureka, Thule and Kiruna. The single large error bar at the left of each panel indicates the estimate of the systematic error on the first data point at each site, which is 12.9% for Eureka and 10% for Thule and Kiruna.

Thule and Kiruna. Day-to-day comparison of SLIMCAT 323 HNO_3 columns with the Eureka lunar and solar columns results in an average difference ((FTIR-SLIMCAT)/FTIR) of −8% for the 20 coincident days, which is within the measurement uncertainty at Eureka. Thus SLIMCAT results are in good agreement with Eureka measurements, while also capturing the observed day-to-day variability. SLIMCAT 323 HNO_3 columns are about 19% higher than both the Thule and Kiruna measurements averaged over the 14 and 25 coincident days, respectively, although SLIMCAT also captures the day-to-day variability observed at Kiruna. SLIMCAT 323 generally reports higher HNO_3 columns than those observed. This is likely due to an overestimate of descent with the new CCMRAD radiation scheme, which appears to be too large for the 2001–2002 winter. SLIMCAT O_3 columns are also slightly too large for this period (not shown), which is consistent with this strong descent.

8. Conclusions

[29] Vertical columns of HNO_3 have been measured for the first time at Eureka using the Moon as a light source. These lunar measurements are in good agreement with the solar values also obtained at Eureka just before and after polar night. This provides us with a consistent HNO_3 time series from fall to spring throughout the polar night. The combination of solar and lunar measurements at Eureka shows a nearly constant increase in HNO_3 values from $\sim 1.8 \times 10^{20}$ molec/m^2 in October to $\sim 3.5 \times 10^{20}$ molec/m^2 at the end of March which is the typical seasonal behavior of HNO_3 in the absence of PSCs and heterogeneous chemistry.

[30] The first comparison of CMAM with HNO_3 observations in the polar regions is presented. CMAM version 7 climatological HNO_3 columns are in good agreement with measurements at Eureka and Kiruna, considering CMAM's small interannual variability. Note that the interannual variability in CMAM version 7 is generally underestimated because there is no quasi-biennial oscillation, solar variability, or aerosol variability taken into account, and the sea surface temperatures are the same in each year of the model's simulation. Also this version of CMAM does not exhibit extremely cold winters, which means no sequestration of HNO_3 in PSCs at these sites. Nevertheless, the comparison reveals that CMAM simulates well the winter buildup and early spring maximum of HNO_3 in the high Arctic during winters without PSCs.

[31] SLIMCAT 323 captures the magnitude of lunar and solar HNO_3 measurements at Eureka as well as the day-to-day variability at Eureka and Kiruna; however SLIMCAT HNO_3 columns are somewhat higher than Thule and Kiruna measurements. This is thought to be due to the strong descent generated by the CCMRAD radiation scheme.

[32] **Acknowledgments.** The Eureka AStrO facility was operated by Meteorological Service of Canada, and the authors are indebted to Jacinta McNairn who spent the entire winter in Eureka recording the lunar FTIR spectra, with dedication and expertise, while also ensuring the operation of the entire AStrO observatory and instruments. The authors are also grateful for the enthusiastic and expert technical assistance rendered by Luc Boudreau from ABB Bomem Inc. in the development of lunar FTIR spectroscopy at the Eureka observatory. The research described here was financially supported by the Meteorological Research Institute of Japan, the Canadian Foundation for Climate and Atmospheric Sciences, the Northern Scientific Training Program, the Canadian Northern Studies Trust, the Natural Sciences and Engineering Research Council of Canada, the Meteorological Service of Canada and the Canadian Space Agency.

References

Austin, J., et al. (2003), Uncertainties and assessments of chemistry-climate models of the stratosphere, *Atmos. Chem. Phys.*, *3*, 1–27.

Beagley, S. R., J. de Grandpré, J. N. Koshyk, N. A. McFarlane, and T. G. Shepherd (1997), Radiative-dynamical climatology of the first-generation Canadian Middle Atmosphere Model, *Atmos. Ocean*, *35*, 293–331.

Blumenstock, T., F. Hase, A. Griesfeller, R. Ruhnke, H. Fischer, U. Raffalski, and Y. Kondo (2003), Chlorine activation, ozone loss and sequestration of nitric acid in PSCs as observed by ground-based FTIR measurements during winter at Kiruna (Sweden) since winter 1993/94, in *Proceedings on the Sixth European Workshop on Polar Stratospheric Ozone*, *Gothenborg 2002*, *Eur. Comm. Air Pollut. Res. Rep.*, *79*, pp. 51–54, Off. for Off. Publ. of the Eur. Commun., Luxembourg.

Chang, Y. S., and J. H. Shaw (1977), A nonlinear least squares method of determining line intensities and half-widths, *Appl. Spectrosc.*, *31*, 213–220.

Chipperfield, M. P. (1999), Multiannual simulations with a three-dimensional chemical transport model, *J. Geophys. Res.*, *104*, 1781–1805.

Chipperfield, M. P. (2006), New version of the TOMCAT/SLIMCAT Off-line Chemical Transport Model, *Q. J. R. Meteorol. Soc.*, *132*, 1781–1805.

Davies, S., et al. (2005), 3-D microphysical model studies of Arctic denitrification: Comparison with observations, *Atmos. Chem. Phys.*, *5*, 3093–3109.

de Grandpré, J., J. W. Sandilands, J. C. McConnell, S. R. Beagley, P. C. Croteau, and M. Y. Danilin (1997), Canadian middle atmosphere model: Preliminary results from the chemical transport module, *Atmos. Ocean*, *35*, 385–431.

Donovan, D. P., et al. (1997), Ozone, column ClO, and PSC measurements made at the NDSC Eureka observatory (80°N, 86°W) during the spring of 1997, *Geophys. Res. Lett.*, *24*, 2709–2712.

Feng, W., et al. (2005), Three-dimensional model study of the Arctic ozone loss in 2002/2003 and comparison with 1999/2000 and 2003/4, *Atmos. Chem. Phys.*, *5*, 139–152.

Goldman, A., C. Paton-Walsh, W. Bell, G. C. Toon, J. F. Blavier, B. Sen, M. T. Coffey, J. W. Hannigan, and W. G. Mankin (1999), Network for the detection of stratospheric change Fourier transform infrared intercomparison at Table Mountain Facility, November 1996, *J. Geophys. Res.*, *104*, 30,481–30,503.

Goutail, F., et al. (2005), Early unusual ozone loss during the Arctic winter 2002/2003 compared to other winters, *Atmos. Chem. Phys.*, *5*, 665–677.

Grooß, J. U., G. Gunther, R. Muller, P. Konopka, S. Bausch, H. Schlager, C. Voigt, C. M. Volk, and G. C. Toon (2005), Simulation of denitrification and ozone loss for the Arctic winter 2002/2003, *Atmos. Chem. Phys.*, *5*, 1437–1448.

Hase, F. (2000), Inversion von spurengasprofilen aus hochaufgelosten bodengebundenen FTIR–Messungen in Absorption, *FZK Rep.*, *6512*, pp. 3417–3422, Forschungszentrum Karlsruhe, Karlsruhe, Germany.

Hase, F., J. W. Hannigan, M. T. Coffey, A. Goldman, M. Hopfner, N. B. Jones, C. P. Rinsland, and S. W. Wood (2004), Intercomparison of retrieval codes used for the analysis of high-resolution, ground-based FTIR measurements, *J. Quant. Spectrosc. Radiat. Transfer*, *87*, 25–52.

Hopfner, M., et al. (1998), The Karlsruhe optimized and precise radiative transfer algorithm, part II: Interface to retrieval applications, *Proc. SPIE Int. Soc. Opt. Eng.*, *3501*, 186–195.

Kanamitsu, M. (1989), Description of the NMC global data assimilation and forecast system, *Weather Forecasting*, *4*, 335–342.

Kopp, G., et al. (2003), Evolution of ozone and ozone related species over Kiruna during the THESEO2000-SOLVE campaign retrieved from ground-based millimeter wave and infrared observations, *J. Geophys. Res.*, *108*(D5), 8308, doi:10.1029/2001JD001064.

Kuntz, M., et al. (1998), The Karlsruhe optimized and precise radiative transfer algorithm, part III: ADDLIN and TRANSF algorithms for modeling spectral transmittance and radiance, *Proc. SPIE Int. Soc. Opt. Eng.*, *3501*, 247–256.

Lait, L., P. Newman, R. Schoeberl (2005), Using the Goddard Automailer, NASA Goddard Space Flight Cent., Greenbelt, Md. (Available at http://code916.gsfc.nasa.gov/Data_services/)

Manney, G. L., K. Kruger, J. L. Sabutis, S. A. Sena, and S. Pawson (2005), The remarkable 2003–2004 winter and other recent warm winters in the Arctic stratosphere since the late 1990s, *J. Geophys. Res.*, *110*, D04107, doi:10.1029/2004JD005367.

Meier, A. (1997), Determination of atmospheric trace gas amounts and corresponding natural isotopic ratios by means of ground-based FTIR spectroscopy in the high Arctic, *Rep. Polar Res.*, *236*, Alfred Wegener Inst. for Polar and Mar. Res., Bremerhaven, Germany.

Meier, A., et al. (2005), Evidence of reduced measurement uncertainties from an FTIR instrument intercomparison at Kiruna, Sweden, *J. Quant. Spectrosc. Radiat. Transfer*, *96*, 75–84.

Murphy, C., et al. (2001), Validation of NDSC measurements of ozone, reservoir compounds and dynamical tracers: Results of a series of side-by-side instrument intercomparisons, paper presented at 2001 Symposium, Network for the Detection of Stratospheric Change, Arcachon, France.

Nash, E. R., P. A. Newman, J. E. Rosenfield, and M. R. Schoeberl (1996), An objective determination of the polar vortex using Ertel's potential vorticity, *J. Geophys. Res.*, *101*(D5), 9471–9478.

Notholt, J. (1994a), The moon as a light source for FTIR measurements of stratospheric trace gases during polar night: Application for HNO_3 in the Arctic, *J. Geophys. Res.*, *99*, 3607–3614.

Notholt, J. (1994b), FTIR measurements of HF, N_2O and CFCs during the Arctic polar night with the moon as light source, subsidence during winter 1992/93, *Geophys. Res. Lett.*, *21*, 2385–2388.

Notholt, J., and R. Lehmann (2003), The moon as light source for atmospheric trace gas observations: Measurement technique and analysis method, *J. Quant. Spectrosc. Radiat. Transfer*, *76*, 435–445.

Notholt, J., R. Neuber, O. Schrems, and T. von Clarmann (1993), Stratospheric trace gas concentrations in the Arctic polar night derived by FTIR-spectroscopy with the Moon as IR light source, *Geophys. Res. Lett.*, *20*, 2059–2062.

Notholt, J., P. von der Gathen, and S. Peil (1995), Heterogeneous conversion of HCl and $ClONO_2$ during the Arctic winter 1992/1993 initiating ozone depletion, *J. Geophys. Res.*, *100*, 11,269–11,274.

Notholt, J., G. Toon, F. Stordal, S. Solberg, N. Schmidbauer, E. Becker, A. Meier, and B. Sen (1997), Seasonal variations of atmospheric trace gases in the high Arctic at 79°N, *J. Geophys. Res.*, *102*, 12,855–12,861.

Peterson, D. B., and J. J. Margitan (1995), *Upper Atmospheric Research Satellite Correlative Measurement Program* (*UARS-CMP*) *Balloon Data Atlas*, NASA, Washington, D. C.

Phillips, D. L. (1962), A technique for the numerical solution of certain integral equations of the first kind, *J. Assoc. Comput. Math.*, *9*, 84–97.

Rinsland, C. P., M. A. H. Smith, P. L. Rinsland, A. Goldman, J. W. Brault, and G. M. Stokes (1982), Ground-based infrared spectroscopic measurements of atmospheric hydrogen cyanide, *J. Geophys. Res.*, *87*, 11,119–11,125.

Rinsland, C. P., A. Goldman, F. J. Murcray, F. H. Murcray, R. D. Blatherwick, and D. G. Murcray (1988), Infrared measurements of atmo-

spheric gases above Mauna Loa, Hawaii, in February 1987, *J. Geophys. Res.*, *91*, 12,607–12,626.

Rodgers, C. D. (1976), Retrieval of atmospheric temperature and composition from remote measurements of thermal radiation, *Rev. Geophys.*, *14*, 609–624.

Rodgers, C. D. (1990), Characterization and error analysis of profiles retrieved from remote sounding measurements, *J. Geophys. Res.*, *95*, 5587–5595.

Rothman, L. S., et al. (1992), The HITRAN molecular database: Edition of 1991 and 1992, *J. Quant. Spectrosc. Radiat. Transfer*, *48*, 469–507.

Rothman, L. S., et al. (2003), The HITRAN molecular spectroscopic database: Edition of 2000 including updates through 2001, *J. Quant. Spectrosc. Radiat. Transfer*, *82*, 5–44.

Sander, S. P., A. R. Ravishankara, and R. R. Friedl (2003), Chemical kinetics and photochemical data for use in stratospheric modeling, update to evaluation 14, JPL Publication, pp. 2–25, NASA Jet Propul. Lab., Pasadena, Calif.

Santee, M. L., G. L. Manney, N. J. Livesey, and W. G. Read (2004), Three-dimensional structure and evolution of stratospheric HNO_3 based on UARS Microwave Limb Sounder measurements, *J. Geophys. Res.*, *109*, D15306, doi:10.1029/2004JD004578.

Schreiber, J., T. Blumenstock, and F. Hase (1997), Application of a radiometric calibration method to lunar Fourier transform IR spectra by using a liquid-nitrogen-cooled high-emissivity blackbody, *Appl. Opt.*, *36*, 8168–8172.

Singleton, C. S., et al. (2005), 2002–2003 Arctic ozone loss deduced from POAM III satellite observations and the SLIMCAT chemical transport model, *Atmos. Chem. Phys.*, *5*, 597–609.

Solomon, S., R. R. Garcia, F. S. Rowland, and D. J. Wuebbles (1986), On the depletion of Antarctic ozone, *Nature*, *321*, 755–758.

Stiller, G. P., et al. (1998), The Karlsruhe optimized and precise radiative transfer algorithm. Part I: Requirements, justification, and model error estimation, *Proc. SPIE Int. Soc. Opt. Eng.*, *3501*, 257–268.

Tikhonov, A. N. (1963), On the solution of incorrectly stated problems and a method of regularization, *Dokl. Akad. Nauk SSSR*, *151*, 501–504.

Toon, G. C., C. B. Farmer, P. W. Schaper, L. L. Lowes, and R. H. Norton (1992b), Evidence for subsidence in the 1989 Arctic winter stratosphere from airborne infrared composition measurements, *J. Geophys. Res.*, *97*, 7963–7970.

Wegner, A., G. P. Stiller, T. von Clarmann, G. Maucher, T. Blumenstock, and P. Thomas (1992), Denitrification and chlorine activation as monitored by ground-based FTIR solar absorption measurements, *J. Geophys. Res.*, *103*, 22,181–22,200.

Wood, S. W., R. L. Batchelor, A. Goldman, C. P. Rinsland, B. J. Connor, F. J. Murcray, T. M. Stephen, and D. N. Heuff (2004), Ground-based nitric acid measurements at Arrival Heights, Antarctica, using solar and lunar Fourier transform infrared observations, *J. Geophys. Res.*, *109*, D18307, doi:10.1029/2004JD004665.

World Meteorological Organization (2003), *Scientific Assessment of Ozone Depletion: 2002*, edited by D. L. Albritton, et al., Geneva, Switzerland.

T. Blumenstock, F. Hase, and S. Mikuteit, Institute of Meteorology and Climate Research, Forschungszentrum Karlsruhe and University of Karlsruhe, D-76021 Karlsruhe, Germany.

M. P. Chipperfield, Institute for Atmospheric Science, School of Earth and Environment, University of Leeds, Leeds LS2 9JT, UK.

M. T. Coffey and J. W. Hannigan, Optical Techniques Project, Atmospheric Chemistry Division, National Center for Atmospheric Research, Boulder, CO 80307, USA.

E. Farahani, C. McLandress, T. G. Shepherd, and K. Strong, Department of Physics, University of Toronto, 60 Saint George Street, Toronto, ON, Canada M5S 1A7. (elham@atmosp.physics.utoronto.ca)

H. Fast and R. L. Mittermeier, Meteorological Service of Canada, Downsview, ON, Canada M3H 5T4.

Y. Makino, Japan Meteorological Agency, Tokyo 100-8122, Japan.

U. Raffalski, Swedish Institute of Space Physics, S-98128 Kiruna, Sweden.